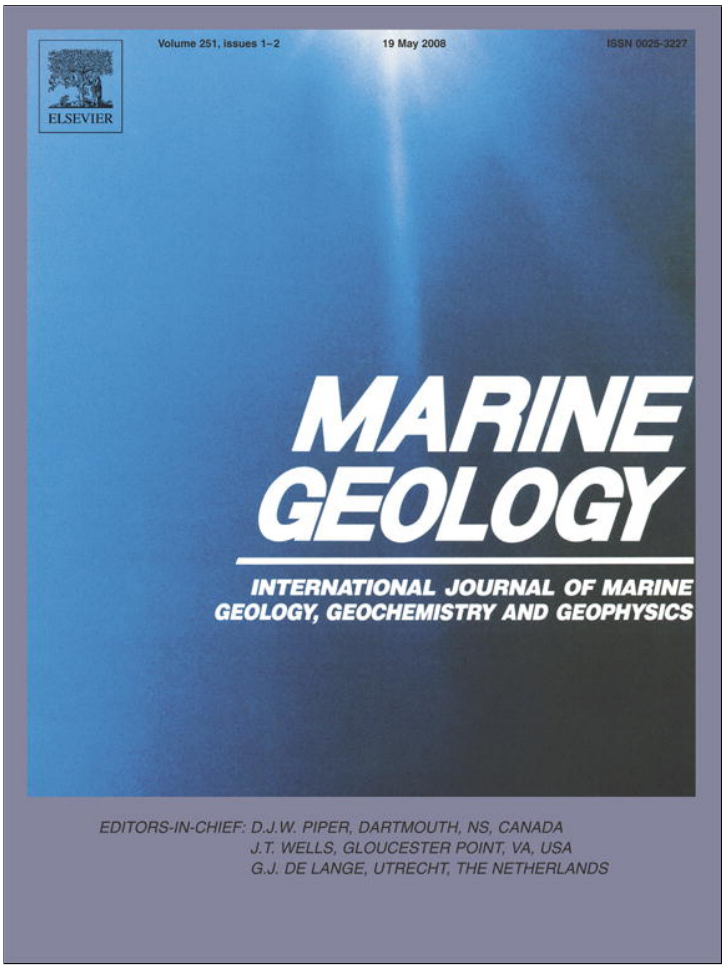

Available online at www.sciencedirect.com
ScienceDirect
Marine Geology 251 (2008) 15–31
MARINE GEOLOGY
INTERNATIONAL JOURNAL OF MARINE GEOLOGY, GEOCHEMISTRY AND GEOPHYSICS
www.elsevier.com/locate/margeo

Turbidites deposited on Southern Central Chilean seamounts: Evidence for energetic turbidity currents

David Völker [a,*], Thomas Reichel [b], Michael Wiedicke [b], Christoph Heubeck [c]

[a] Leibniz-Institut für Meereswissenschaften an der Universität Kiel (IFM-GEOMAR), Wischhofstr. 1-3, D-24148 Kiel, Germany
[b] Bundesamt für Geowissenschaften und Rohstoffe, Stilleweg 2, D-30655 Hannover, Germany
[c] Institut für Geologische Wissenschaften der Freien Universität Berlin, Malteserstr. 74-100, D-12249 Berlin, Germany

Received 12 February 2007; received in revised form 23 January 2008; accepted 24 January 2008

Abstract

Gravity cores obtained from isolated seamounts located within, and rising up to 300 m from the sediment-filled Peru–Chile Trench off Southern Central Chile (36°S–39°S) contain numerous turbidite layers which are much coarser than the hemipelagic background sedimentation. The mineralogical composition of some of the beds indicates a mixed origin from various source terrains while the faunal assemblage of benthic foraminifera in one of the turbidite layers shows a mixed origin from upper shelfal to middle-lower bathyal depths which could indicate a multi-source origin and therefore indicate an earthquake triggering of the causing turbidity currents. The bathymetric setting and the grain size distribution of the sampled layers, together with swath echosounder and sediment echosounder data which monitor the distribution of turbidites on the elevated Nazca Plate allow some estimates on the flow direction, flow velocity and height of the causing turbidity currents. We discuss two alternative models of deposition, both of which imply high (175–450 m) turbidity currents and we suggest a channelized transport process as the general mode of turbidite deposition. Whether these turbidites are suspension fallout products of thick turbiditic flows or bedload deposits from sheet-like turbidity currents overwhelming elevated structures cannot be decided upon using our sedimentological data, but the specific morphology of the seamounts rather argues for the first option. Oxygen isotope stratigraphy of one of the cores indicates that the turbiditic sequences were deposited during the last Glacial period and during the following transition period and turbiditic deposition stopped during the Holocene. This climatic coupling seems to be dominant, while the occurrence of megathrust earthquakes provides a trigger mechanism. This seismic triggering takes effect only during times of very high sediment supply to the shelf and slope.

Keywords: turbidity current; suspension fallout; bedload deposit; Peru–Chile Trench; perched turbidite beds; turbidity current runup; mass wasting

1. Introduction

Turbidite deposits on positive submarine bathymetric features (seamounts, ridges) that are separated from the probable source regions of the turbidites by a larger distance and deep water such as trenches or abyssal plains witness high-energy sediment deposition processes. Sand-sized turbidity current deposits in perched positions have been documented from submarine ridges, including the Hawaiian Arch (Garcia and Hull, 1994), the Tiburon Rise (Dolan et al., 1989a,b), the Mediterranean Ridge (Cita et al., 1984), and seaward flanks of submarine trenches, such as the Aleutian Trench (Underwood, 1987) and the Middle America Trench (Moore and Watkins, 1982). In the case of ODP Site 842 on the Hawaiian Arch, where turbidity currents travelled at least 240 km from the source and ran up the Hawaiian Arch to a maximum run-up elevation of 500 m, turbidity currents were generated by giant submarine landslides at the flanks of the Hawaiian Islands (Garcia and Hull, 1994). Turbiditic beds deposited on the Tiburon Rise in the central Atlantic Ocean have been interpreted to be the products of turbidity currents of extreme thickness (500–1500 m), derived from northern South America, more

* Corresponding author. Tel.:+ 49 431 600 2566.
E-mail address: dvoelker@ifm-geomar.de (D. Völker).

0025-3227/$ - see front matter © 2008 Elsevier B.V. All rights reserved.
doi:10.1016/j.margeo.2008.01.008

than 1000 km away (Dolan et al., 1989a,b). A specific explanation for these turbidity currents, extreme in terms of run-up elevation and surpassed distance was not given. In the case of the Aleutian Trench, thin sand layers which originated from the Alaska Peninsula were found on the seaward side of the trench, 1000–2400 m above the trench axis. In any of the cited cases, authors were cautious about deciding whether the run-up elevation is to be seen as indicator of the height of the currents, or, alternatively, currents of a height less than the run-up moved uphill.

Muck and Underwood (1990), from arguments of energy exchange, establish a relation between the thickness of a turbidity current h, and the maximum run-up elevation y_{max}, which the flow can surmount when it meets a given barrier at right angle. They state that $h > 1.08\ b/(2-E_{loss})$ [1], E_{loss} being the dimensionless energy loss of the flow due to friction at the seafloor and b being the height of the barrier. Assuming an energy loss of 33%, the author's first-order approximation is $y_{max} = 1.53\ h$ [2], which proved adequate in laboratory experiments. The calculation of a minimum height of the flow allows for an estimation of the maximum flow velocity u using a numerical expression of Muck and Underwood (1990), which describes the exchange of kinetic energy for potential energy during upslope flow: $0.50\ U^2(1-E_{loss}) = (\Delta\rho/\rho)\ g\ y_{max}$ [3]. $\Delta\rho$ is the density contrast between the turbid liquid and seawater with $\rho = 1024$ g/cm^3, g is the gravitational acceleration.

In the case of central Chile (35–42°S), several causes and trigger mechanisms for sedimentation events, able to mobilize large volumes of sediment and to affect a certain depth range of the continental margin, are possible: (1) the high seismicity of the Chilean continental margin and in particular the occurrence of megathrust earthquakes with magnitudes Mw > 8 at a recurrence rate of 100–350 yr (e.g. Cisternas et al., 2005) makes earthquakes a possible candidate for triggering the failure of sediments of the continental slope. We assume that giant earthquakes occurred with about the same frequency during Pleistocene as today, because the rate of convergence between the Nazca Plate and the South American Plate was similar (Pardo-Casas and Molnar, 1987); (2) a close correlation between the temporal frequency of turbiditic events which produce seismic reflectors in the sediments of the Peru–Chile Trench and climatic (Milankovic) cycles has been reported by Rauch (2005). Thus, some form of climatic triggering of turbidity currents seems likely, but the way by which turbidite deposition is related to climatic changes is not yet clear. (3) The loss of the stabilizing effect of gas hydrates on continental margins during sea-level low-stand, and, as a consequence, the generation of "mega-turbidites" has been discussed for other continental margins (Rothwell et al., 1998). A bottom-simulating reflector (BSR) indicating the existence of gas hydrates is visible in many seismic profiles along the Chilean continental margin from 33°S to 44°S (Brown et al., 1996; Grevemeyer et al., 2003). Two seismic profiles of Grevemeyer et al. (2003) fall into the area under discussion and show a BSR which is almost continuous from ~1500 m water depth to > 3000 m water depth (Fig. 1).

The criteria for distinguishing earthquake-triggered turbidite deposits (seismoturbidites) sedimentologically from other types of turbiditic deposits are still strongly debated (Goldfinger et al., 2003). Nakijama and Kanai (2000) and Shiki et al. (2000) propose such criteria should include (1) a wide areal extent of the deposits, (2) variable provenance, (3) multi coarse fraction pulses and (4) unusually great volume of the resulting turbidites.

The purpose of this study is to describe and quantify sedimentation processes which led to the deposition of sand layers on seamounts in the Chile Trench and to find evidence about their cause and trigger mechanism. In order to do so, we examine the sandy beds in terms of grain size and sedimentary structures, which, together with the position of the sites, is used as a proxy for velocity and flow height of the causing turbidity current. Additional information about the distribution of turbidites and the possible turbidity current pathways is drawn from acoustic data (sediment echosounder and swath echosounder). Components of the coarse fraction of one of the beds are examined for clues about the possible source region. One of the cores was dated in order to link the events to the climate history of South America.

2. Regional setting

2.1. Bathymetry

The continental margin of Southern Chile between 36°S and 39°S is characterized by a shelf of intermediate width (20–30 km) with a shelf edge at 150–250 m. The continental slope is inclined at 2.5°–4.0° with frequent irregularities such as plateaus, slope basins and escarpments as steep as 10°. The slope is dissected by four major and some minor deeply incised meandering submarine canyons (Biobío, Imperial, Tolten and Calle-Calle) connected to large rivers. The Paleo–Pellahuen Canyon seems to be a relict feature of the Pellahuen River. According to Rehak et al. (2008), this river, which now forms a tributary to Rio Imperial, once reached the Pacific before being deflected by uplift in the Nahuelbulta segment of the Coastal Cordillera. Some of the canyons begin directly at the mouths of the corresponding rivers (e.g. Biobío and Calle-Calle) and cut into the shelf. They should therefore effectively funnel long-shore transported sediment as well as fluvial input downslope. The canyons (namely the Biobío Canyon) end in submarine fans where they enter the trench (Thornburg and Kulm, 1990). The Biobío fan is most pronounced, whereas the Tolten and Calle-Calle fans appear as relicts of formerly larger features (Völker et al., 2006).

Between the Juan Fernandez Ridge at 32°30′S and the Chile Ridge at 46°S, the Peru–Chile Trench is filled by 2.0–2.5 km of predominantly turbiditic sediment (Bangs and Cande, 1997; Reichert, 2002; Ranero et al., 2006). Due to this infill, the trench appears as a flat plain of 25–70 km width, adjacent to the lowermost slope. It is inclined to the North with a slope angle of 0.12°.

In the trench, a 7–10 km wide and about 150 m deep, slightly sinuous axial channel is observed. It originates from the Chacao Canyon at 41°S, is connected to the exits of the largest submarine canyon systems of the continental margin (Calle-Calle, Tolten, Biobío and San Antonio Canyons) and is

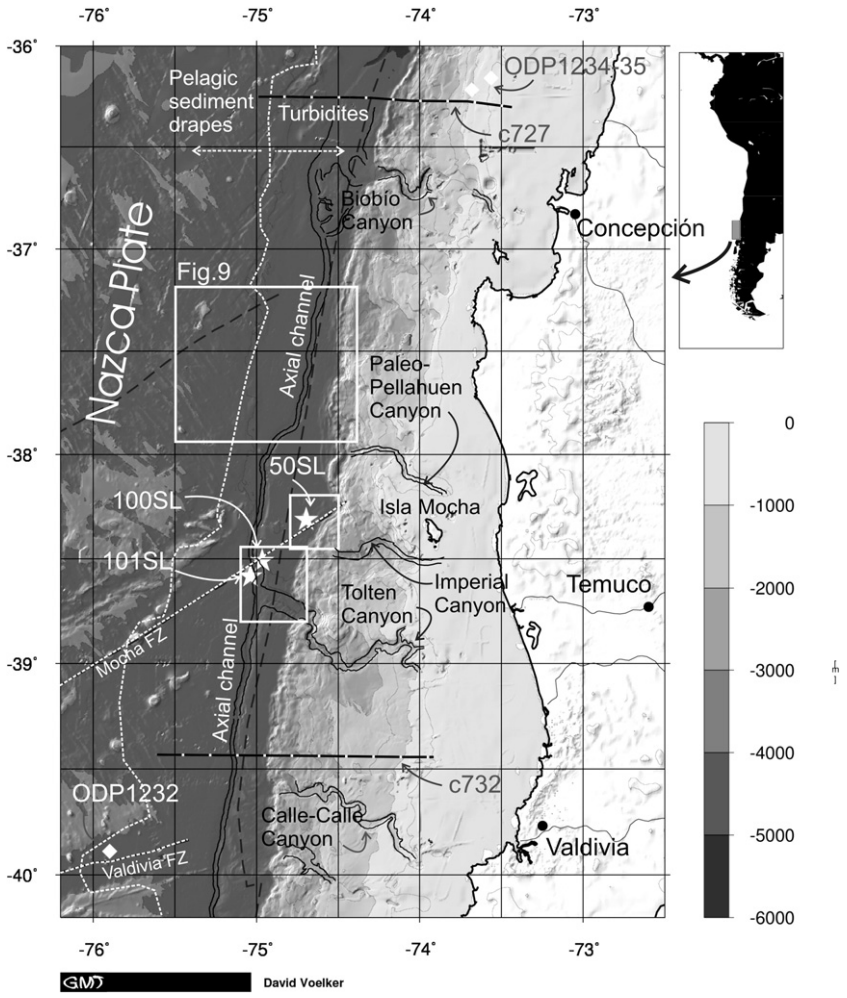

Fig. 1. Bathymetry of the continental margin, the Peru–Chile Trench and the Nazca Plate off Chile (36°S–40°S). The bathymetry was compiled from swath echosounder data of various *RV SONNE* cruises. The seaward limit of the turbiditic infill of the trench is indicated as dotted white line. It was extrapolated from sediment echosounder survey data. Positions of detail maps of Figs. 2, 3 and 9 are indicated as boxes. Gravity core stations and ODP sites are indicated as stars and diamonds. Major submarine canyon systems and the axial channel of the Peru–Chile Trench are delineated. The positions of these features were extracted from swath bathymetry data of *RV SONNE* cruise SO161. Seismic profiles c727 and c732, cited in Grevemeyer et al. (2003) show a Bottom Simulating Reflector.

traceable across the Juan Fernandez Ridge swell at 32°S (Thornburg and Kulm, 1990; Laursen and Normark, 2002; Völker et al., 2006). Some canyons are connected to this channel by a single connecting feeder channel (as in the case of the Tolten Canyon) or by distributary channels winding through the sediment fan (as in the case of the Biobío and Calle-Calle Canyons). At 35°35′S, a detached, coherent slump mass (olistolith) of ~95 km^2 extent partly buries the channel (Völker and Weinrebe, 2006).

The bulge of the Nazca plate forms the seaward boundary of the trench. It is elevated 100–400 m with respect to the filled trench and shows parallel lineaments which delineate the spreading fabric. The Nazca Plate carries chains of up to 2 km high seamounts aligned sub-parallel to the Valdivia and Mocha Fracture Zones (Fig. 1). As the seamounts approach the subduction zone and the underlying crust subsides, they are progressively buried by trench sediments. The tops of buried seamounts form isolated hills in the trench. Three of these hills were selected for gravity core sampling (Fig. 1).

2.2. Sedimentation

At present, terrigenous sediment input into the sea occurs mainly by rivers in the sector of the Chilean coast between 33°S and 43°S (Lamy et al., 1998). The rate of sediment supply is related to the precipitation at the western flank of the Andes, which shows a pronounced latitudinal gradient with high rainfall in Southern Chile (200–800 cm/yr) and intermediate to low rainfall (100 cm/yr) northwards at Valparaiso (New et al., 1999). The larger rivers (Biobío and Calle-Calle) emerge from the Andes, cross the central valley of Chile and cut through the Coastal Cordillera. As the area represents the transition from temperate to glacial climate zones, Pleistocene climatic changes have caused extensive fluctuations of glaciation (Rabassa and Clapperton, 1990) which very likely affected sediment supply to the trench significantly (Bangs and Cande, 1997).

ODP site 1232, (Leg 202, Mix et al., 2003), was drilled at the seaward side of the sediment-filled Peru–Chile Trench, 85 km west of the lowermost continental slope (Fig. 1). The uppermost

362 m are Pleistocene sediments and consist of gray silty clay and clay, interbedded with numerous (>800) graded layers of silty sand, partly with sharp basal contacts. The silty sand layers were interpreted as basal parts of distal turbiditic deposits. They contribute to 22% of the uppermost 20 m of the sequence and range in individual thickness from a few cm to 108 cm. Both lithologies, the clay beds as well as the interbedded graded sand beds show a mineral assemblage which is consistent with andesitic source rocks of the Southern Andes. The stratigraphy of the cored sequences indicates very high overall sedimentation rates (>450 m/My, possibly much higher in the upper section), resulting in a high frequency of turbidite events on the order of 1 event per century. The thickness of individual turbidite layers (>1 m) suggests large turbidity current events.

A prominent oceanographic feature of the area with relevance to the sedimentation on the continental slope is the double oxygen minimum zone (OMZ) with oxygen minima at 400 m and 1500 m water depths (WOCE, 2002). These water masses, depleted in oxygen (<150 μmol/kg water) are related to the high-productivity upwelling zones off northern Chile and Peru.

3. Methods

The sediment cores were obtained in 2002 during expedition SO161-5 of the German *RV SONNE*. The sampling tool for sediment cores was a 1.5 t gravity corer which retrieves cores with a diameter of 10 cm. The cores were described on board.

Grain size distribution analysis of prominent beds was performed with a liquid laser-particle analyser (Galai CIS-100). Individual beds were sampled each cm. Five cm^3 of sample material were suspended in 100 ml of deionised water plus 1 ml of 1 M NH_4-solution. The sediment suspension was split and each of the subsamples was analysed independently, determining particle sizes between 0.5 and 600 μm. The interval <10 μm was measured in steps of 1 μm, from 10 to 100 μm in steps of 10 μm, and between 100 and 600 μm in steps of 50 μm. We did not take the precaution to remove foraminifera from the subsamples prior to grain size analysis, therefore single shells could bias the size distribution in individual subsamples. Nevertheless, this effect seems to be neglegible as the measurements on various subsamples always gave reproducible curves. In general, foraminifera were rare and we had to sieve 50–100 cm^3 to obtain a representative number.

Foraminifera were picked from the >125 μm fraction and mounted on EM-carriers for photographic documentation with a Zeiss Scanning Electron Microscope (DSM 960 A). The benthic foraminifera were then identified by comparison with publications covering the Peru–Chile Trench area (Bandy & Rodolfo, 1964; Ingle et al., 1980). As certain species are characteristic of different environments (e.g. dissolved oxygen, temperature) they were related to water masses and respective water depths.

The mineral assemblage was examined using thin sections of grain mounts. The fresh sediment material was wet-sieved with a 63 μm sieve; the residual sediment was dried and fixed with resin for the final grain mounts. The thin sections were then studied for mineral content.

Oxygen isotopic composition was determined using the planctonic foraminifera *Globigerina bulloides*. The samples were extracted from the core in 10 cm intervals. We chose only samples which were taken from fine-grained intervals (background sedimentation) avoiding possible turbidite beds.

The analysis was done using a Thermo Finnigan Kiel III carbonate preparation device connected to a ThermoFinnigan 252 mass spectrometer. The tests were dissolved in 100% phosphoric acid (H_3PO_4, Wachter and Hayes, 1985), the CO_2 which is set free was automatically trapped, frozen and directly passed to the mass spectrometer. All values are reported in per mil (‰) relative to V-PDB. Reproducibility was checked by replicate analysis of laboratory standards ($\delta^{18}O$ 1σ <0.08‰). The resulting curves were then graphically correlated with marine standard oxygen isotope curves (Martinson et al., 1987).

For accelerator mass spectrometry (AMS) ^{14}-C analyses we used 8–11 mg of tests of planktonic foraminifera. Samples were analysed at the Leibniz Laboratory, University of Kiel. Results are given in Fig. 8. Conversion to calendar years was achieved applying a reservoir age correction of 580 yr (Shackleton et al., 1988) and using the radiocarbon calibration software CALIB (Rev. 5.0.2) following Stuiver et al. (2005) and Hughen et al. (2004).

Along the track of *RV SONNE* cruises 161-3 and 161-5, sediment echosounder profiling was performed with the sediment echosounder PARASOUND (Krupp Atlas Elektronik, e.g. Hübscher et al., 1997). Good profiles were obtained in the sediment-filled graben and on the Nazca Plate, whereas the continental slope and the seamounts were too steep for coherent echo return. PARASOUND data were digitized and recorded with the data acquisition system PARADIGMA (Spiess, 1993).

During cruise legs 161-1 to 161-5, the SIMRAD EM 120 multibeam echosounder was operated. The signal frequency is 12 kHz; signals are emitted as an array of 191 single beams, covering a swath angle of up to 150°. The cruise tracks were designed to obtain sufficient coverage, which resulted in a bathymetric data set of good quality and extent. We integrated the cruise data into a bathymetric grid with the MB-System Tools software (Caress & Chayes, 1995, 1996). The resulting bathymetric maps of the core location areas (Figs. 2 and 3) are based on a ~200 m grid and were produced with the Generic Mapping Tools (GMT) software of Wessel and Smith (1998).

4. Results

4.1. Core description and grain size distribution

During cruise leg SO161-3 (Wiedicke et al., 2002) three gravity cores, SL50, SL100 and SL101 (from N to S) were recovered from the summits and flanks of three unnamed seamounts within the Peru–Chile Trench (Figs. 1, 2, 3). The cores sampled 7.32 m (SL50), 3.90 m (SL100) and 3.28 m (SL101) of the seamount sediment sequence. The material was classified as clayey mud, muddy clay and muddy pelletal sands grading into silty clay interbedded with numerous thin graded black sand layers (Wiedicke et al., 2002). The sand layers have sharp bottom contacts, are massive or partly laminated and can

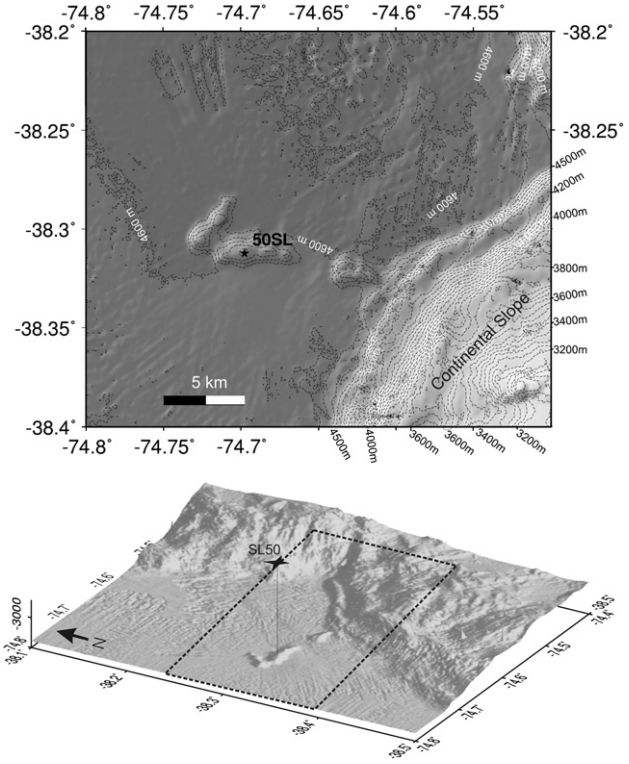

Fig. 2. Map and perspective view of the coring location of sediment gravity core SL50 8.5 km west of the base of the continental slope in the Peru–Chile Trench (38°18.75′S 74°41.85′W, 4380 m water depth). The coring site lies on the summit of an elongate seamount, 200 m above the surrounding abyssal plain, between the exits of the Imperial and the Paleo–Pellahuen Canyon.

be macroscopically identified by their dark colour and coarse composition.

1) Core SL50: The coring site lies on top of a small, elongate seamount which rises 200 m from the surrounding abyssal plain, the site is 8.5 km west of the subduction front (Fig. 2). We counted 36 individual graded sandy beds. Most have a thickness of 1–4 cm, with two exceptional beds found in the depth intervals 37–42 cm and 54–58 cm. These beds stand out visually because of their thickness, darkness, and comparatively large grain size (Fig. 4). The grain size distribution of the sampled layers proves grading of the beds.

Interval 37–42 cm contains 36.9 vol.% of grains in the size range 100–150 μm and 18.25 vol.% of grains within the range of 150–200 μm at 39 cm core depth (Fig. 4). The cumulative percentile value of 50% or median, D_{50}, increases downcore from the top of the bed at 37 cm to a maximum at 39 cm and decreases further downcore (see Fig. 4a, b). The maximum value of D_{50} is 110 μm. The basal contact of the bed, which is observed visually is less clearly represented by the data, maybe due to bioturbation. The background sedimentation is represented by the cumulative grain size curve at 42 cm depth (D_{50} value 18 μm).

Interval 54–58 cm contains 32.31 vol.% of grains in the size range 100–150 μm and 17.46 vol.% of grains within the range of 150–200 μm at 58 cm core depth (Fig. 4d). This is in striking contrast to the intervals between sandy beds which show their maxima of ~25% in the interval 10–20 μm. The interval shows a constant downcore increase of D_{50} from 55 μm to 105 μm. The basal layer contains 32.3 vol.% grains in the range 100–150 μm.

2) Core SL100: The coring site is situated on top of a cone-shaped seamount which rises 270 m from the surrounding abyssal plain, 20 km west of the subduction front. It lies directly landward of the axial channel (Fig. 3). We recognized some thicker individual turbidite beds and a high number of thin (<1 cm) and fine turbidite beds which were homogenized by bioturbation. We sampled the most prominent beds at the depth intervals of 304–306 cm, 338–341 cm, 350–352 cm and 370 cm. They consist mainly of coarse silt and thus are much finer grained and less distinct from the background sedimentation than the turbidite beds of core SL50 (Fig. 5a–c).

3) Core SL101: The coring site lies in a central, horseshoe-shaped depression of a seamount, 23.5 km away from the subduction front. The northern rim of this crater-like structure rises 600 m from the surrounding abyssal plain. The coring site is elevated 150 m in respect to the abyssal plain seaward of the seamount and 300 m in respect to the floor of the axial channel (Fig. 3). The axial channel lies landward of the seamount, where

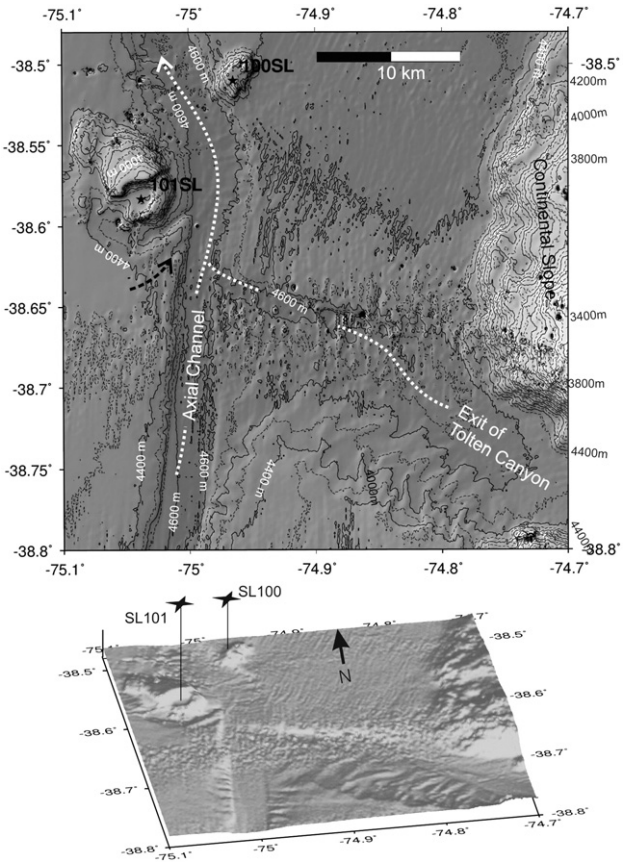

Fig. 3. Map and perspective view of coring location of sediment gravity cores SL100 (38°30.60′S 74°57.90′W, 4223 m) and SL101 (38°35.00′S 75°02.27′W, 4298 m) in the Peru–Chile Trench. The central axial channel is cut 150 m into the trench fill. Another channel connects the exit of the Tolten Canyon to the axial channel. The channel walls show scouring structures, e.g. where the channel coming from the Tolten Canyon exit joins the axial channel (black dashed arrow). The white arrows indicate the most probable ways of channelized turbidity currents.

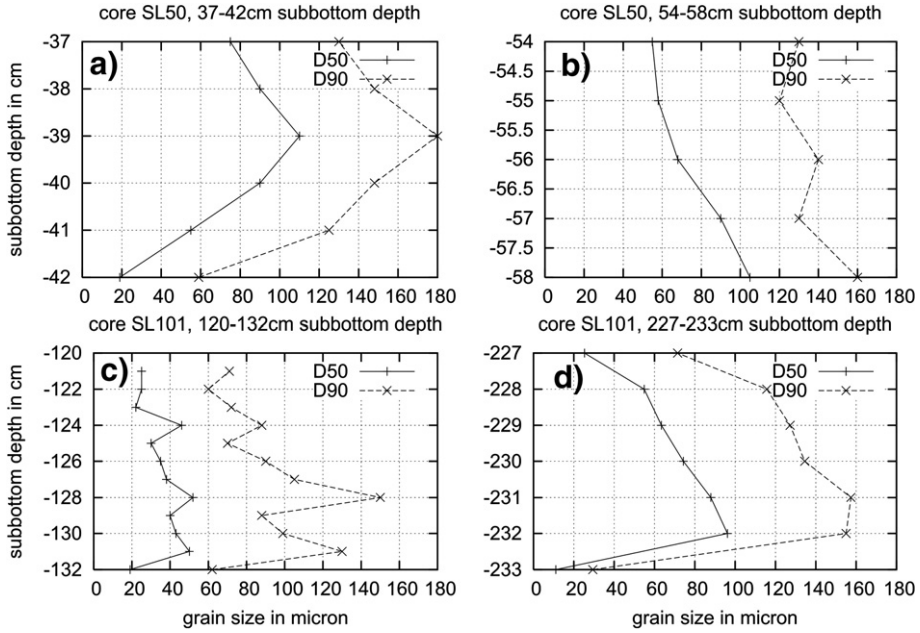

Fig. 4. Grain size variations (mean grain size, D_{50} and 90 Percentile D_{90}) within visually prominent turbiditic layers of gravity cores SL50 and SL101. The interval 37–42 cm of SL50 exhibits an increase in mean grain size from 37 cm to 39 cm. The base of this particular bed is not very sharp which may be due to bioturbation. The interval 54–58 cm shows a clear grading with a maximum mean grain size of 103 μm at the base. In core SL101, interval 120–132 shows a succession of thin turbidites, whereas interval 227–233 shows a sharp base and clear grading upwards.

it intersects with a channel that connects to the Tolten Canyon exit. The core exhibits black sandy beds at the depth intervals of 120–131 cm, 227–232 cm, 290–292 cm and 309–310 cm as well as some thin, discontinuous black sand layers.

The interval 120–132 cm is a thick, rather uniform layer. It is coarser than the background sedimentation above and below, but not as coarse as interval 227–233 cm (Fig. 6a). Grading is indicated by a downcore trend in median grain size from 30 mm to 55 μm but not continuous (Fig. 4c). It has a higher density as the background as is recorded by a sharp drop in the gamma ray core log.

Interval 227–233 cm shows a plane-parallel (tb-) bedding and a sharp contact at the base. The lowermost part of the turbidite contains abundant fine sand (33.97 vol.% in the range 100–150 μm). In the interval, grading is obvious, as the median of the samples increases downcore from the top of the bed (227 cm depth, 25 μm mean grain size) to the base of the layer (232 cm depth, 100 μm mean grain size, Fig. 4d). The sharp basal contact of the bed is shown by the sudden drop of the mean grain size to about 15 μm below (233 cm), which represents the grain size distribution in the background sedimentation intervals between sandy beds (Fig. 4d).

Altogether, the most prominent beds by thickness and grain size are intervals 037–042 cm and 054–058 cm in core SL50 and 228–233 cm in core SL101. Less prominent in terms of elevated median grain size but conspicuous by its thickness is interval 120–132 cm in SL101.

In Fig. 5 we plotted the D_{50} mean grain siza and the 90 percentile (D_{90}) of all samples of the sampled sandy beds against the distance to the lower continental slop, the distance to the axial channel and the elevation of the coring site relative to the trench floor.

4.2. Mineralogy of a coarse grained bed in core SL50

The mineralogy of the >63 μm fraction of the 37–42 cm interval of core SL50 show (1) *felsic volcanic material* such as volcanic glass with flow structures and gas inclusions, partly deglassing, trachytic plagioclase laths, single large feldspars and tourmaline, (2) *sedimentary and metamorphic clasts* such as thin-shelled and agglutinating foraminifera tests, metamorphic quartz, mono-crystals of calcite, anchimetamorphic shale clasts, rounded sedimentary clasts and (3) *mafic volcanic material* such as pyroxene, mica flakes and microcrystalline chlorite. Table 1 represents the analysis of a binocular grain count.

4.3. Benthic foraminifera in core SL50

The samples of the turbidite layers of core SL50, interval 37–42 cm contain few, but diagnostically significant benthic and planctonic foraminifera (Fig. 7). We use the established relationship between water depth and/or dissolved oxygen concentrations and the relative abundances of several species of benthic foraminifera in sedimentary environments to determine the primary depositional depths of the reworked components (e.g. Bernhard, 1986; Ingle et al., 1980; Kaiho, 1991; Kaiho, 1994; Schmiedl et al., 1998). The composition of benthic foraminifers' assemblages varies, but many contain shallow water species.

Typical representatives of the outer-shelf biofacies (135–150 m water depth) are *Nonion mexicanum* (Williamson), *Cassidulina sp.* and *Trifarina angulosa* (Williamson, Fig. 7). In particular *Cassidulina minuta* is typical for the shallow oxygen minimum fauna (~1.5 ml/l) of the continental margin of Chile (Ingle et al., 1980).

Globobulimina affinis (d'Orbigny) and *Uvigerina peregrina* (Cushman) are members of the upper bathyal biofacies (Ingle et al.,

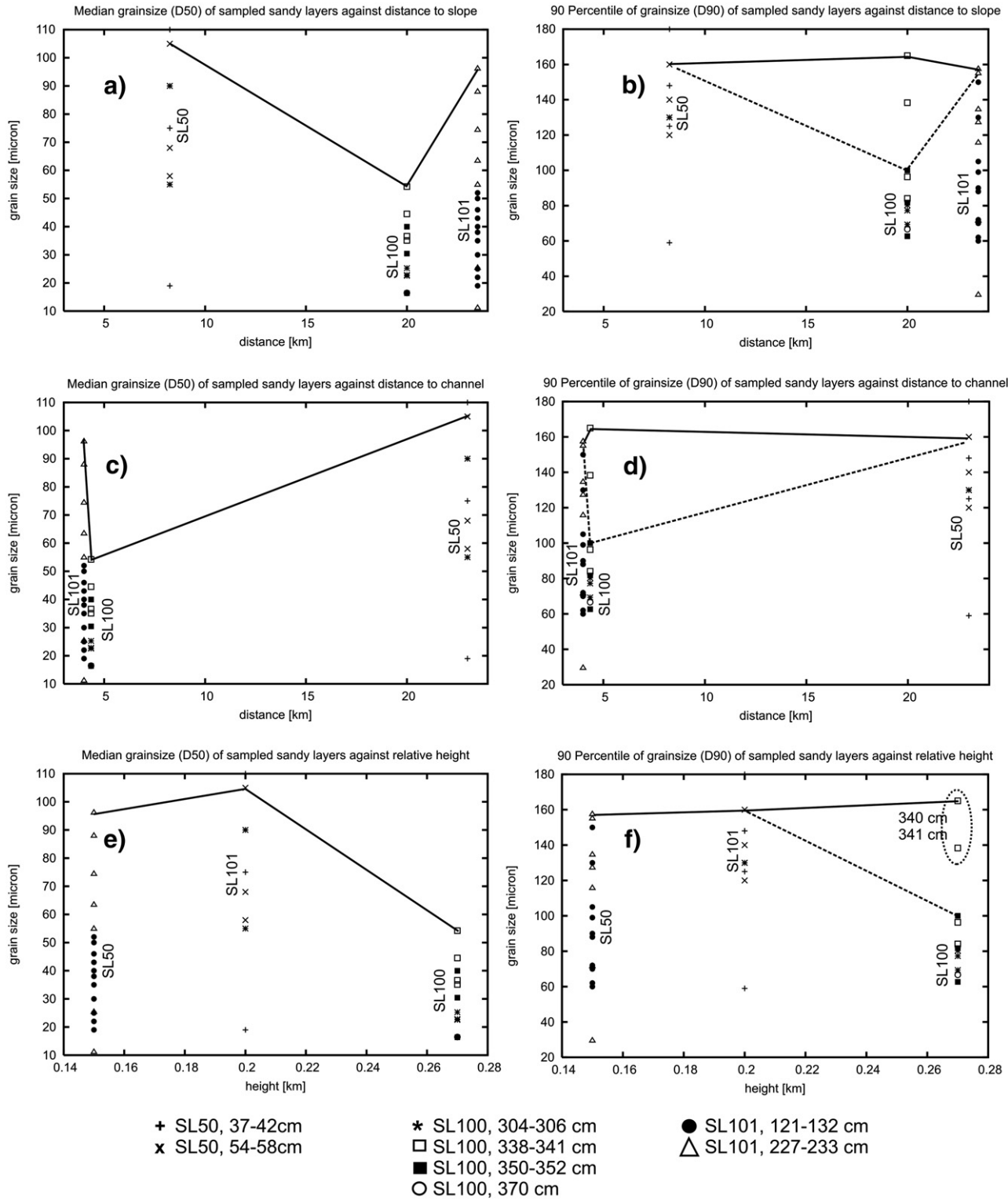

Fig. 5. Grain size distribution (D_{50} and D_{90}) of all samples in relation to the site's distance to the lower continental slope (a–b), the distance to the axial channel (c–d) and the elevation of the coring site relative to the trench floor (e–f).

1980) and are associated with dissolved oxygen contents lower than ~3 ml/l and a depth-distribution between 150 and 500 m.

Uvigerina hispida (Schwager) is typical and abundant in sediments from water depths between 500 and 1500 m. Off Chile this water depth range comprises an oxygen-rich upper part (500–900 m, the Antarctic Intermediate Water) and an oxygen-depleted lower part (900–1500 m). *Uvigerina hispida* (Schwager) is characteristic for the latter.

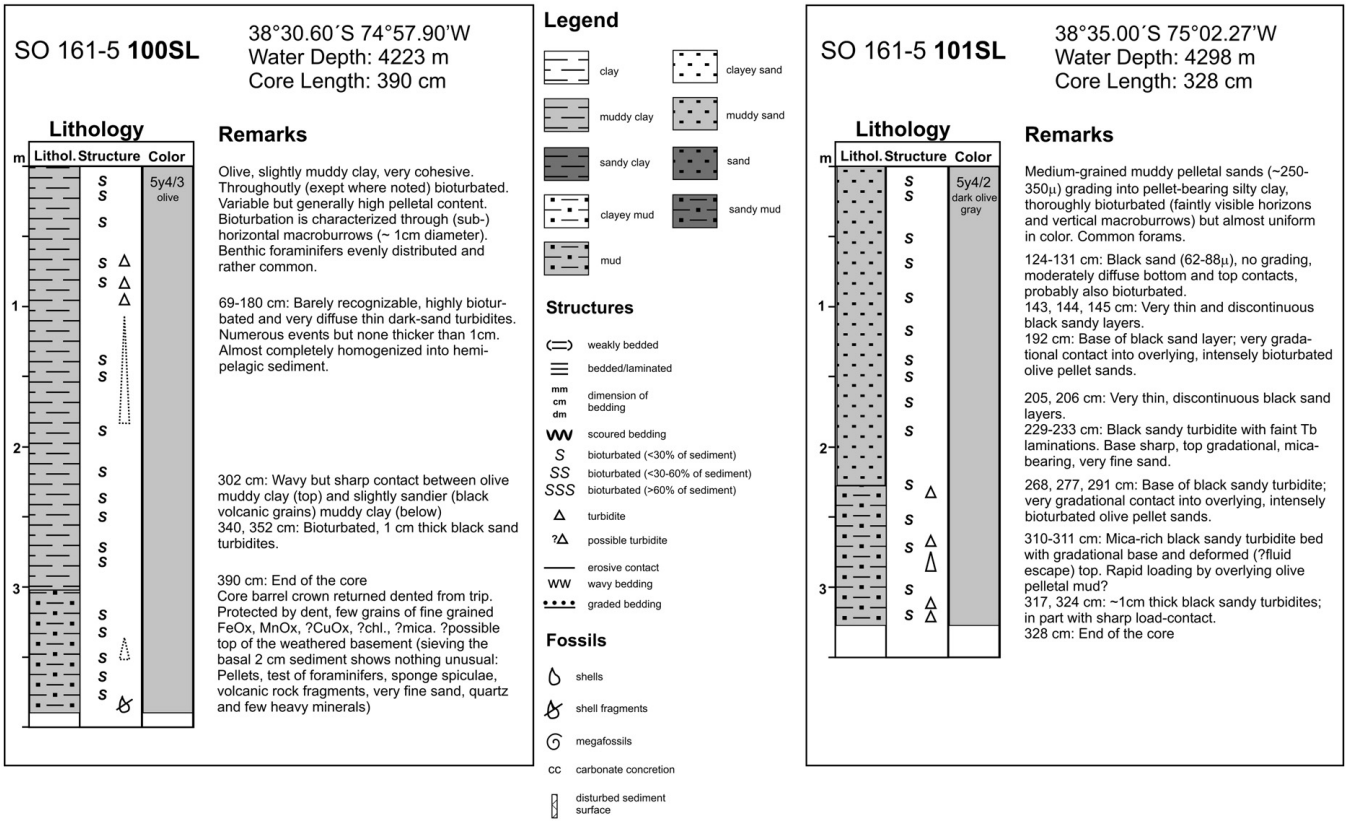

Fig. 6. Commented core description log of gravity cores SL100 and SL101.

Table 1
Estimation of volume percentage of mineral components of the 63 μm fraction of a turbidite layer (38–41 cm interval) in gravity core SL50

Depth of core	38 cm	39 cm	40 cm	41 cm
Poorly sorted, fine-grained sandy siltstone	40	35	45	50
Quartz: volcanic, polycrystalline	10	15	5–10	5–10
Plagioclase	10	10	5–10	<5
Glauconite pellets	<5	<<5	<5	<5
Volcanic Lithoclasts-andesitic	20	20	20	30
Calcite	<<5	10		
Calcite (fossil fragments, including forams)	<5	<5	<5	<5
Metamorphic quartz–sericite–schist	10	10	<5	<<5
K-feldspar	?	<<5	<5	?
Zircon	?	<<5	<5	?
Pellets, unspecified	<5	<<5	<5	5
Chert	?	?	<<5	?
Opaque	<5	<5	<<5	5
Glass	?	<<5	<<5	<<5

The lower middle bathyal biofacies (1500–2000 m water depth) is represented by *Bulimina barbata* (Cushman), one of the index species for this depth (Ingle et al., 1980).

4.4. Age of turbidites in SL50

Most of the core SL50, from the base at 7.32 m–1.5 m core depth, exhibits a relatively uniform and fairly heavy oxygen isotope signal in the range of 2.5–3.5‰ (Fig. 8). This pattern can be related to the last glacial period (MIS2). From 1.5 m core depth to the top of the core there is a sharp decrease of $d^{18}O$ values from 3.0‰ to 0.7‰. This decrease is interpreted to represent the global warming of the atmosphere after the last glaciation and is very similar to the MIS2 to Holocene section of the $\delta^{18}O$ curve derived from the Vostok ice cores (Bender, 2002) and the marine standard oxygen isotope curve of Martinson et al. (1987). This is supported by the two AMS^{14}C ages (see Fig. 8). The topmost 30 cm of the core SL50 represents the Holocene time period. The relation in thickness between the Holocene section and the more than 5 m (minimum) thick glacial section suggest that sedimentation rates were significantly higher during the glacial than during the Holocene time period. The two thick turbidite layers described above fall into the transition period between glacial and Holocene and are about 8–13 ka old.

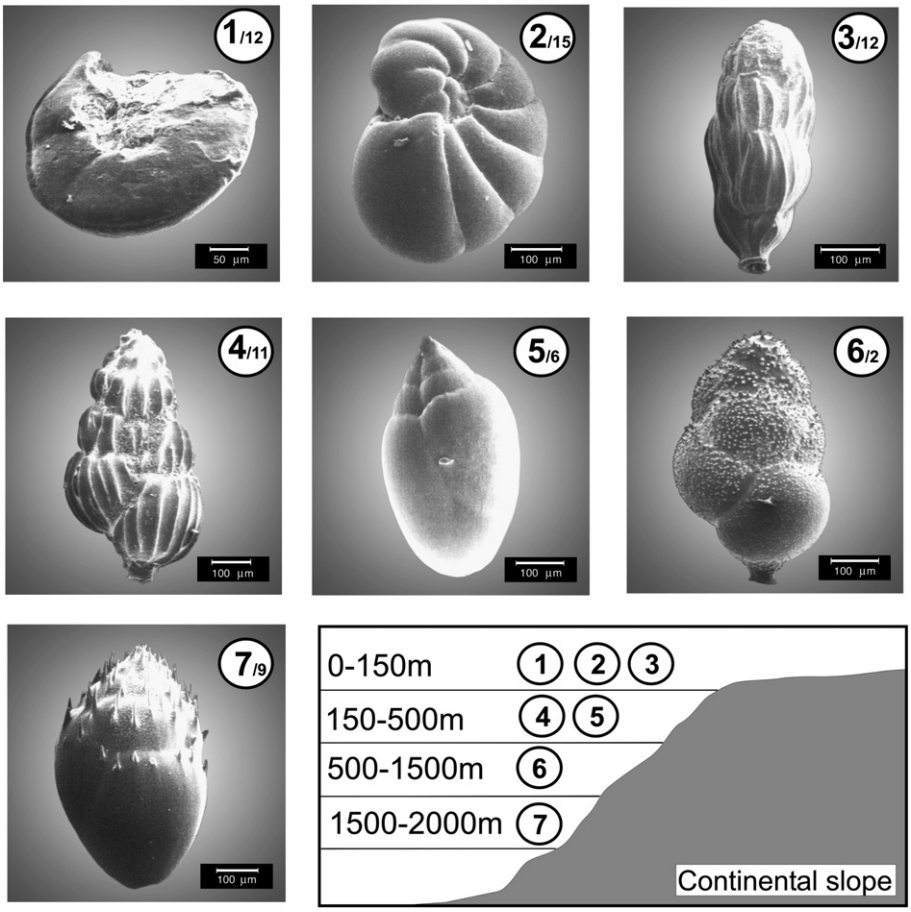

Fig. 7. Foraminifera species within the basal layer of turbidite bed layer within core SL50 (037–042 cm bsf). The different species are related to certain depth ranges and oxygen concentration ranges, as discussed in the text. The small numbers give the respective number of counted specimens. *Cassidulina minuta*; Cushman, 1933, Cushman Lab. Foram. Res., Contr., Vol. 9, pt. 4, p. 92. pl. 10, Fig. 3. *Nonion mexicanum*; Williamson=*Nonion turgidus*; Williamson, avr. Mexicanus Cole, 1927, Bull. Amer. Pal. Vol. 14, No. 51, p. 23, pl. 2, Fig. 11. *Trifarina angulosa* Williamson, 1858, Recent foraminifera of Great Britiain, Royal Soc., London, p.67, pl. 5, Fig. 140. *Uvigerina peregrina*; Cushman, 1923, US. Nat. Mus. Bull., No. 104, 166, xlii, 7–10. *Globobulimina affinis d'Orbigny=Bulimina affinis* D'Orbigny; 1839, in de la Sagra, Hist. Phys. Pol. Nat. I'lle Cuba, Foraminifères, p.105, pl.2, Fig. 25–26. *Uvigerina hisipida*; Schwager, 1866, Novara-Exped., Geol., Theil., Vol. 2, pt. 2, p. 249, pl. 7, Fig. 95. *Bulimina barbata*; Cushman, 1927, Calif. Univ. Scribbs Inst. Oceanogr., Bull., Techn. Ser., Vol..1, no.10, p.151, pl.2, Fig.11.

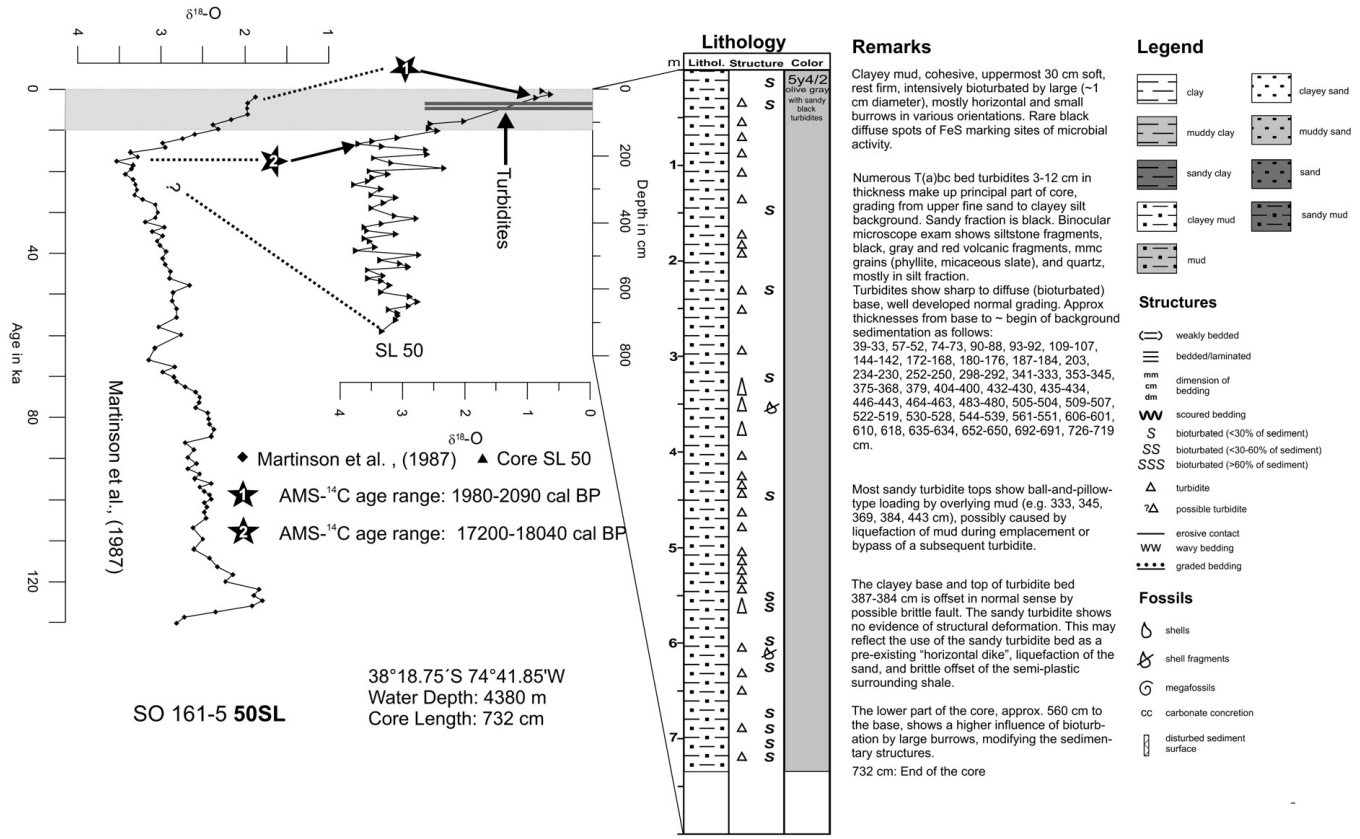

Fig. 8. Correlation of oxygen isotope data of planctonic foraminifera of core SL50 with standard oxygen isotope curve (Martinson et al., 1987) and lithological description.

4.5. Acoustic facies and bathymetry around the coring sites

Sediment echosounder (Parasound) profiles across the trench and the adjacent Nazca Plate show few, easily distinguishable echo patterns. In the trench, seawards as well as landwards of the central axial channel, profiles show low signal penetration (10–40 m) and indistinct energy return. This acoustic character is produced by a high number of flat-lying, semi-parallel, densely spaced internal reflectors which are continuous for several kilometres (Fig. 9a). In the following we call this kind of reflection pattern *type A* for convenience. A similar pattern with higher signal penetration (60–70 m) is observed to the south of Biobío and Tolten Canyon exits. Low signal penetration and, in places, small hyperbolic echoes are observed within the central axial channel within distributary channels which emerge from the canyon exits and north of the Biobío canyon exit.

The topographic gradient of the trench fill is very low with the exception of the axial channel and the fan systems and distributary channels related to the submarine canyon systems of Tolten and Biobío. The axial channel cuts up to 150 m into

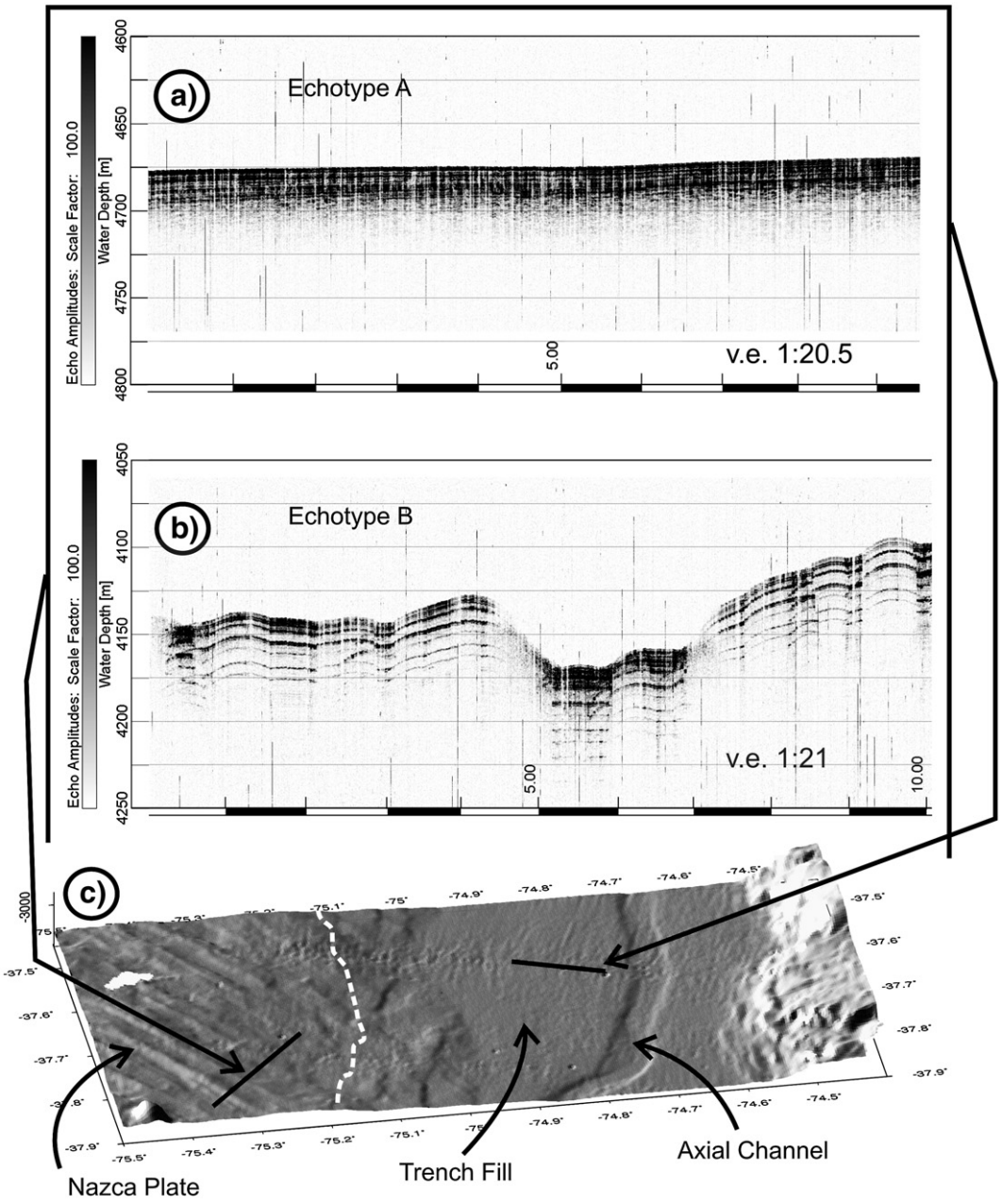

Fig. 9. Parasound-echosounder profiles from the Peru–Chile Trench and Nazca Plate. a) Profile located within the trench fill. The trench floor as well as subbottom reflectors are generally horizontal. Densely spaced sub-parallel reflectors give an indistinct energy return to a depth of no more than 30 m (echotype A). b) Image of sediments on the Nazca Plate seawards of the Peru–Chile Trench. Undulating parallel reflectors indicate sediment beds of uniform thickness (pelagic drapes). The signal penetration reaches 50 m (echotype B). The seaward limit of type A and the transition to type B mark the seaward termination of continent-derived turbidites as they onlap on the pelagic strata of the Nazca Plate (dotted line gives approximate location).

the sediments, truncating reflectors at the channel walls (Völker et al., 2006). In places, the channel walls are scarred by gullies, slumps and scouring structures, e.g. where the Tolten fan feeding channel joins the axial channel (Fig. 3). There is no systematic difference in the height of both of the shoulders of the axial channel.

The seaward limit of the flat trench fill is marked by the fairly rough topography of the Nazca Plate. Its surface displays a characteristic linear topographic pattern caused by the crustal horst- and graben-structure which is masked only by a relatively thin hemipelagic cover (Wiedicke et al., 2002, Fig. 9c). Acoustically, this cover is characterized by evenly spaced, continuous and very distinct reflectors (Fig. 9b). We will afterwards term this characteristic reflection *type B*. These reflectors are parallel to each other follow the undulating seafloor surface. The signal penetration is significantly higher (70–100 m) than within the trench sediments.

The direct transition between both echo types is rarely resolved in our profiles due to hilly topography, but we can draw a line between the patchy occurrences of both. This line lies at a defined height of 200 m above mean trench depth and 350 m above the floor of the axial channel. Seismic images with deeper penetration (Reichert and SPOC Scientific Shipboard Party, 2002; Ranero et al., 2006) show that the transition is time transgressive as is indicated by the progressive onlap of the horizontally stratified trench sequence on the undulating drapes of the Nazca Plate.

Acoustic data show no indication of contourites, mudwaves or other sedimentary features of the seafloor indicative of enhanced bottom water currents. This implies generally low bottom water velocities, probably on the order of only a few cm/s.

5. Discussion

5.1. Identification of turbidite beds

The grain size analysis shows that the beds, sampled at elevated positions within the trench, have high content of fine to medium sand (Wentworth, 1922) which contrasts with the very fine-grained background sedimentation. In many cases (most clearly in bed 227–233 cm of core SL101, Fig. 4d and bed 54–58 cm of core SL50, Fig. 4b), beds show pronounced grading upwards as well as sharp bottom contact and sedimentary structures including a plane-parallel (tb-) bedding and thus are clearly turbidite beds. In other sandy layers, grading is less convincing which we attribute to bioturbation after deposition and succession of thin turbidites (Fig. 4a,c).

5.2. Grain size distribution and site position

If the grain size distribution of the sampled sandy beds is related to the position of the coring sites, e.g. if the value of D_{90} or D_{50} is plotted against the site's distance to the deformation front (assuming a source on the slope and a free flow from the east to the west across the trench, Fig. 5a–b), or against the site's distance to the axial channel (assuming a channelized flow within the axial channel from the south to the north, Fig. 5c–d), no uniform trend is detected which could help us to decide upon the possible transport direction (Fig. 5a–d, solid line). This observation is surprising as one should expect the transport capacity of turbidity currents to decrease in a region of low gradient with distance from the source. Probably the distance between the sites is too small to have a marked effect upon the grain distribution. This is an argument in favor of turbidity currents which are horizontally homogeneous across the trench width.

If the grain size distribution is related to the site's height relative to the trench floor, a general trend can be seen as sand layers in SL50 (200 m relative height, 8.5 km distance to slope) and SL101 (150 m relative height, 23.5 km distance to the slope) are rather similar in their grain size distribution and thickness, whereas silt and sand layers in SL100 (270 m relative height, 20 km distance to slope) have a much more distal character. This is reflected in the drop of D_{50} from 200 to 270 m height (Fig. 5e). It is less well visible in the D_{90} curve, because the only thicker bed of core SL100 (338–341 cm) has a D_{90} value comparable to beds of the other sites (Fig. 5f, encircled). This bed is unique to core SL100 and may represent an atypical single event, whereas the majority of detectable turbidite layers in the interval 69–180 cm have D_{90} values <60 μm. If we exclude this bed as a singular event, the D_{90} curve shows the same height dependency as for D_{50} (Fig. 5f, dotted line), which indicates that the height of the obstacle indeed produces a grain size sorting effect between 200 and 270 m but not between 150 and 200 m. If we eliminate bed 338–341 cm of SL100 in the grain size vs. distance plots (Fig. 5b and d, dotted lines), no other but the mentioned height relation becomes visible.

5.3. Distribution of turbidites within the trench

The distribution of turbidites and the upper reach of the turbiditic depositional environment is imaged by the acoustic data. Echo type A (Fig. 9a) is typical for the trench sediments with a relatively high content of silt and sand in thin beds, representing distal turbidites (sheet turbidite deposits). Echo type B (Fig. 9b) was found at the area of the hilly topography of the Nazca Plate. As can be seen in seismic profiles (Reichert and SPOC Scientific Shipboard Party, 2002; Ranero et al., 2006; Rauch, 2005), this bathymetry is caused by the crustal horst- and graben-structures of the Nazca Plate which is masked by a predominantly hemipelagic cover of ~150 m thickness. This echotype monitors sedimentation processes which are independent of the seafloor topography, as younger reflectors mimic the shape of the preceding deposits (sediment drapes).

The transition from echo types A to B (shown as dashed line in Figs. 1, 9 and 10) thus delimits the westward and upward turbiditic depositional environment. According to the position of this line, turbidity currents spill out into the trench and cross the axial channel. After travelling over essentially flat grounds for 50–80 km turbidite beds settle on the bulging Nazca plate, 200 m above the mean depth, respectively 350 m above the maximum depth of the trench, the axial channel.

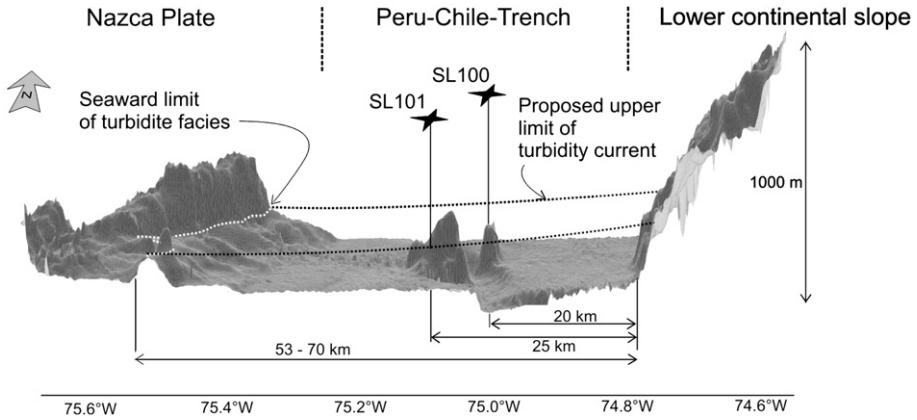

Fig. 10. Perspective view of the continental slope, trench and Nazca Plate and spatial extent of a hypothetical unchannelized turbidity cloud, able to produce turbidite beds at coring sites SL100 and SL101 and turbidite beds on the seaward wall of the Peru–Chile Trench.

5.4. Estimates on height and velocity of the turbidity current

5.4.1. Unchannelized flow

When we use a first-order approximation (Eq. (9) of Muck and Underwood 1990, herein cited as Eq. (1)), we obtain a minimum thickness h of the turbidity current of ~175 m for SL100. The extent of such a turbidity cloud is illustrated in Fig. 10. When we take this height and calculate a density of the flow by assuming a grain density range of 2000–2500 kg^{-3}, a combination of the Eq. (1) and of Muck and Underwood (1990, herein cited as Eq. (3)) and their empirical relation (herein cited as Eq. (2)) give the following results for the maximum flow velocity u of the turbidity current: with a concentration of 9% of sediment by volume, which is considered an upper limit for true turbidity currents by Mulder and Alexander (2001), u would be 11–13 m/s. A flow of 5% of sediment by volume would still require 8.2–10 m/s and a flow of 1% of sediment by volume would require 3.6~4.4 m/s.

The velocity values lie in the range of or exceed those obtained for channelized turbidity currents in submarine canyons by direct observation or by calculation from cable breaks (Scripps Canyon, 1.9 m/s, Shepard et al., 1979; Zaire Submarine Canyon, 1.21 m/s, Khripounoff et al., 2003; Var Canyon, 1.8–7 m/s, Piper and Savoye, 1993), or by modelling (Amazon Canyon, 0.5–4 m/s, Pirmez and Imran, 2003). On the other hand, they are lower than those calculated for the erosive turbidites following the Grand Banks slope failure event (16.6–27.7 m/s, Fine et al., 2005, at least 19 m/s, Piper et al., 1988). Piper et al. (2007) showed that turbidity currents resulting from the Grand Banks event turned from being erosive to being depositional only after a considerable slowdown of the turbidity current (initial velocity >19 m/s). As the turbidity currents this manuscript deals with deposited sand, velocities much less than 10 m/s and therefore sediment concentrations less than 5% are probable.

5.4.2. Channelized flow

The Coriolis effect should produce an asymmetry in the lateral deposition from channelized turbidity currents (e.g. Komar, 1969, Piper and Savoye, 1993). Bowen et al. (1984) used the asymmetry in the maximum height above the channel axis to which turbidites were deposited (mean cross-flow slope) to estimate flow velocity. We cannot perform an analogous calculation for the axial channel using our sites SL100 and SL101, because the respective height of the coring sites is not necessarily the maximum height of turbidite deposition. Also we did not find sediment waves which we could interpret in terms of flow velocity.

Klaucke et al. (1998) used height differences of the lateral levees of the Northwest Atlantic Mid-Ocean Channel to infer velocity variations of channelized turbidity currents over time. In the case of the axial channel, we cannot observe a systematic asymmetry in the height of both channel shoulders, nor do cross profiles show the typical (wedge-shaped) geometry of levees produced by long-term flow stripping (e.g. Hübscher et al., 1997; Klaucke et al., 1998). From these observations we can conclude that either (1) the axial channel is a relatively young and predominantly erosive feature which has cut into pre-existing sheet turbidite layers or (2) most of the trench fill has to be considered as levee deposits which would argue for sediment clouds with a height that exceeds the channel depth (150 m) by far, in order to be able to distribute settling sediment in the observed homogeneous way within the trench.

5.5. Composition of selected beds

Examinations of the components of the sand-sized fraction of a thick turbidite bed of core SL50 shows an assemblage of benthic foraminifera, which cannot be related to an in-situ community at ~4000 m water depth. The abundance of *Cassidulina sp.*, and *Uvigerina hispida* (Schwager) is a signal for oxygen-deficient water conditions, which do not prevail at the sampling site. Instead, we see a mixed assemblage including upper and lower slope species from 500 to 2000 m water depth. The rock components have a mixed source with volcanic rock fragments which have a mineralogical composition with a close affinity to the alkaline volcanic rocks of the Andean hinterland, as well as sedimentary and metamorphic clasts which were probably derived from the Western Series formation of the Coastal Cordillera (Martin et al., 1999; Willner, 2005). This composition, in particular the presence of metamorphic clasts

and the absence of basaltic material, also clearly excludes the possibility that the turbidites were generated locally on the same seamount.

The mixture of components of various depths of the continental slope implies that sediment from upper to lower slope has been incorporated into a single bed. A very local slope failure (point source) e.g. at the upper slope most likely generates a turbidity current confined to one of the canyons; it is unlikely to supply such a diversity of components to the turbidity current and to generate the described turbidite bed in the trench. In this aspect, the most prominent bed in SL050 satisfies at least one of the criteria proposed by Shiki et al. (2000) for seismoturbidites with line sources and/or multiple sources.

5.6. Alternative deposition models

Two depositional models for the observed sediment beds are likely: 1) turbidity currents, generated by mass wasting events on the open continental slope, which cross the trench and axial channel and spread westward onto the Nazca Plate (unconfined turbidity currents), or, 2) turbidity currents which emerge from the slope or in the canyon heads, are funneled by the submarine canyons, delivered to and at least partly guided by the axial channel from south to the north (channelized turbidity currents).

Both cases imply turbidity currents which carry fine sand to a height of 150 m, and silt to a height of 270 m above the trench floor (resp. 300 m and 420 m above the axial channel floor) and to a distance of 25 km from the slope and another 30–40 km further to the west, onto the Nazca Plate (Fig. 1, dotted line). The deposition could be either from a flow which had the momentum to overcome the respective height difference by "climbing uphill" or by settling from a thick turbidity current (-"cloud") with a flow height exceeding the height difference to the coring sites. Dolan et al. (1989a,b) used estimates on the angle at which the Tiburon Rise as an elongate barrier was hit by turbidity currents to decide upon this alternative. As they suggest a flow parallel to the contours of the rise, momentum-induced upslope flow would be at a minimum and consequently they favor settling from a thick (600–1500 m) turbidity current. Garcia and Hull (1994) propose an uphill-flow model for their slump-generated turbidity currents to overtop the 500 m high Hawaiian Arch which is met by the currents roughly at right angle. In our case, the approximately conical seamounts form an obstacle to turbidity currents, no matter if they come from the west (unconfined transport) or from the south (channelized transport), but they should have much less effect on the current than an elongate barrier met at right angle, because the flow can bifurcate and flow around them.

5.6.1. Unconfined turbidity currents

The minimum thickness of unchannelized turbidity currents would have to be 175 m in order to move uphill to site SL100 and deposit silt there. The range of the maximum flow velocity u (as calculated in 5.4) is somewhat lower than for the Grand Banks event, which serves us as an example for an unchannelized turbidity current generated by a large slope failure event (volume of 200 km^3). Still, values are reasonable and slope failure events of smaller volume (about 10–20 km^3) are described from Southern Central Chile (Völker and Weinrebe, 2006). The diverse composition of the thick turbidite bed in SL50 is an argument in favor of a wide depth range of the source area or multiple sources. On the other hand, transverse (E–W) sediment transport seems unlikely for several reasons. First, the axial channel and its tributaries are definitely northward-directed transport structures. Transverse transport would gradually fill and erase the axial channel, but it appears as a fully preserved, erosive structure along its course from 41°S to 32°S, except for 35°35′S, where it is partly covered by debris of a lower slope mass wasting event (Völker and Weinrebe, 2006). Also the "drainage" network of the submarine canyons and their tributaries and the general slope bathymetry make it highly probable that turbidity currents which evolve from the upper or middle slope are either caught within one of the major canyons on the way to the trench and delivered into the axial channel or ponded into one of the slope basins.

5.6.2. Turbidity currents guided by the axial channel

The alternative model would imply that turbidites are generated on the upper slope, guided by the submarine canyons and fed into the axial channel. Deposition would be by overspill or by fallout out of a turbidity cloud which is by far higher than it's actively eroding lower portion. As there is no marked difference in bathymetry and seismic facies between both sides of the axial channel and within the trench, turbidite beds seem to be distributed in a homogeneous way 30–40 km to both channel sides. Erosive structures are exclusively found within, and on the western shoulder of the channel (Völker et al., 2006). From these observations we conclude that the flow thickness (or height of the sediment cloud) has to exceed the channel depth by at least another 200–300 m (totalling 350–450 m) and that the erosive lower part of the flow is confined to the channel. Pirmez and Imran (2003) showed that the grain size of levee deposits of the Amazon Channel varies with the height of the flow, with the sandy portion of the flow being restricted to a height of 20–30 m above the channel axis and a marked decrease in the median grain size above that. As we find median sand at site SL101 at 300 m above the channel floor, the energy, volume and flow height of the respective turbidity currents has to exceed those of the lower Amazon Channel.

In this alternative model, the composition of the thick turbidite bed in SL50 would have to be explained by a mixing of provenances in the canyon head. This is not unlikely as the rivers that feed the system traverse different terrains and receive much of the longshore transported sediment. In addition, sediment from the middle slope would have to be incorporated in a growing turbidity current.

5.7. Dating and implications for causes and triggers

Exact timing of the layers was difficult because of scarcity of planctonic foraminifera. For the same reason we were not able to correlate single turbidite layers across the area. As a general trend, core SL50 contains a climatic signal indicating a decrease of high-

energy turbidite sedimentation with the onset of global warming after the last glaciation. We therefore propose that the turbiditic record is related to the climatic record as suggested by Rauch (2005). Whether the climate coupling is due to fluctuations of the sealevel and, as a consequence, in the distance between coast and shelf edge, (de)glaciation of the Andes or reorganisation of the gas hydrate stability zone cannot yet be decided upon. The very thick (>1 m) turbidite beds detected at ODP site 1232 adds to our impression that large depositional events were common during Pleistocene. The climatic coupling which we see in SL50 and the absence of Holocene turbidite beds in spite of the historic record of giant earthquakes in Southern Central Chile leads us to speculate that megathrust earthquakes may play a role as ultimate trigger of mass wasting events but not as a determining cause. In fact, the recurrence rate of giant earthquakes of some centuries as observed in Chile could even be a limiting factor, as the slopes are shaken vigorously in intervals which allow the accumulation of large sediment masses only at times when sedimentation rates are extremely high — as for example during rapid glacial retreats. During these times, however, the turbidite pulse could be directly linked to the earthquake cycle, as the historic recurrence time of large seismic events (Cisternas et al., 2005) and the frequency of Pleistocene turbidites observed at ODP site 1232 (Leg 202, Mix et al., online) are similar (0.5–1 per century).

To further eludicate the ultimate causes of the large turbiditic events reported here, it would be necessary to date, correlate, and map the extent of turbiditic beds in similar perched positions such as on the bulge of the Nazca Plate in order to estimate volumes of single events and tie them to the climatic record. A detailed stratigraphy of ODP core 1232 of leg 202 could provide a reference section. On the other hand, it would require to scan the continental slope of Central Chile for morphological features that witness past mass wasting events such as slump headscarps and failed masses on the lower slope. New swath bathymetry data which were obtained on RV METEOR cruise M67 indeed show a number of suspicious morphological features which will be analysed soon. Establishing links between the sedimentary record of large sediment transport events in the trench and on the slope should be the future goal.

6. Conclusions

Three gravity cores which were obtained on isolated seamounts located in the sediment-filled Peru–Chile Trench off Southern Central Chile (36°S–41°S) contain turbiditic beds composed of particles from a variety of sources and water depths. These beds were formed by settling from thick turbidity currents exceeding the height of the seamounts which originated from the Chilean continental margin. The specific composition of beds may point towards a multi point-source origin which would be an argument for seismically triggered slope failures (seismoturbidites).

Two models are proposed: (1) sedimentation from unchannelized turbidity currents generated by mass wasting on the open continental slope, transport downslope and westwards across the trench or (2) sedimentation from turbidity currents which are funneled via the submarine canyons and guided northwards by the axial channel. We favor the second option as the general mode, without excluding the first for single, major events like the one that produced an olistolith in the trench or exceptional beds. The turbidity currents had a minimum flow height of 350–450 m, extended across the width of the trench (40 km) and were homogeneous laterally as well as up to a height of 200 m.

The stratigraphic record indicates a decrease of high-energy turbidite sedimentation with the onset of global warming after the last glaciation. We speculate that the frequency of turbidite events is linked to the recurrence of giant earthquakes with a rate of some centuries during phases of very high sedimentation on the continental slope, such as during Late Pleistocene, whereas both are decoupled at present.

Acknowledgments

We wish to thank the scientific party of cruise SO161 and the crew of *RV SONNE* for their support. The data this work is based on were obtained within the framework of German research programs SPOC (Subduction Processes off Chile), TIPTEQ (from the Incoming Plate to Megathrust Earthquakes) and the Collaborative Research Centers SFB267 and SFB574. This publication is contribution no. 144 of the Sonderforschungsbereich 574 “Volatiles and Fluids in Subduction Zones” at Kiel University.

Appendix A. Supplementary data

Supplementary data associated with this article can be found, in the online version, at doi:10.1016/j.margeo.2008.01.008.

References

Bandy, O.L., Rodolfo, K.S., 1964. Distribution of foraminifera and sediments, Peru–Chile Trench Area. Deep-Sea Res. 11, 817–837.

Bangs, N.L., Cande, S.C., 1997. Episodic development of a convergent margin inferred from structures and processes along the southern Chile margin. Tectonics 16, 489–503.

Bender, M., 2002. Concentration and Isotopic Composition of O_2 and N_2 in Trapped Gases of the Vostok Ice Core. National Snow and Ice Data Center. Digital media, Boulder, CO.

Bernhard, J.M., 1986. Characteristic assemblages and morphologies of benthic foraminifera from anoxic, organic-rich deposits: Jurassic through Holocene. J. Foraminiferal Res. 16, 207–215.

Bowen, A.J., Normark, W.R., Piper, D.J.W., 1984. Modelling of turbidity currents on Navy Submarine Fan, California Continental Borderland. Sedimentology 31 (2), 169–185.

Brown, K.M., Bangs, N.L., Froelich, P.N., Kvenvolden, K.A., 1996. The nature, distribution, and origin of gas hydrate in the Chile Triple Junction region. Earth Planet. Sci. Lett. 139 (3–4), 471–483.

Caress, D.W., Chayes, D.N., 1995. New software for processing sidescan data from sidescan-capable multibeam sonars. Proceedings of the IEEE Oceans 95 Conference, pp. 997–1000.

Caress, D.W., Chayes, D.N., 1996. Improved processing of Hydrosweep DS multibeam data on the R/V Maurice Ewing, Mar. Geophys. Res. Lett. 18, 631–650.

Cisternas, M., Atwater, B.F., Torrejon, F., Sawai, Y., Machuca, G., Lagos, M., Eipert, A., Youlton, C., Salgado, I., Kamataki, T., Shishikura, M., Rajendran, C.P., Malik, J.K., Rizal, Y., Husni, M., 2005. Predecessors of the giant 1960 Chile earthquake. Nature 437 (7057), 404–407.

Cita, M.B., Beghi, C., Camerlenghi, A., Kastens, K.A., McCoy, F.W., Nosetto, A., Parisi, E., Scolari, F., Tomadin, L., 1984. Turbidites and megaturbidites from the Heredotus abyssal plain (eastern Mediterranean) unrelated to seismic events. Mar. Geol. 55, 79–101.

Dolan, J.F., Beck, C., Ogawa, Y., 1989a. Upslope deposition of extremely distal turbidites: an example from the Tiburon Rise, west-central Atlantic. Geology 99, 990–994.

Dolan, J.F., Beck, C., Ogawa, Y., Klaus, A., 1989b. Eocene–Oligocene sedimentation in the Tiburon Rise/ODP Leg 110 area: an example of significant upslope flow of distal turbidity currents. In: Mascle, A., Moore, J.C. (Eds.), Initial Reports of the Ocean Drilling Program, vol. 110B. Ocean Drilling Program, College Station, Texas.

Fine, I.V., Rabinovich, A.B., Bornhold, B.D., Thomson, R.E., Kulikov, E.A., 2005. The Grand Banks landslide-generated tsunami of November 18, 1929: preliminary analysis and numerical modeling. Mar. Geol. 215 (1–2), 45–57.

Garcia, M.O., Hull, D.M., 1994. Turbidites from giant Hawaiian landslides: results from Ocean Drilling Program Site 842. Geology 22, 159–162.

Goldfinger, C., Nelson, C.H., Johnson, J.E., 2003. Holocene earthquake records from the Cascadia subjection zone and Northern San Andreas fault based on precise dating of offshore turbidites. Annu. Rev. Earth Planet. Sci. 31, 555–577.

Grevemeyer, I., Diaz-Naveas, J., Ranero, C.R., Villinger, H.W., Ocean Drilling Program Leg 202 Scientific Party, 2003. Heat flow over the descending Nazca plate in central Chile, 32°S to 41°S: observations from ODP Leg 202 and the occurrence of natural gas hydrates. Earth Planet. Sci. Lett. 213 (3–4), 285–298.

Hübscher, C., Spiess, V., Breitzke, M., Weber, M., 1997. The youngest channel–levee system of the Bengal Fan: results from digital sediment echosounder data. Mar. Geol. 141, 125–145.

Hughen, K., Lehman, S., Southon, J., Overpeck, J., Marchal, O., Herring, C., Turnbull, J., 2004. 14C activity and global carbon cycle changes over the past 50.000 years. Science 303, 202–207 (and supporting online material).

Ingle, J.C., Keller, G., Kolpack, R.L., 1980. Benthic foraminiferal biofacies, sediments and water masses of the southern Peru–Chile Trench area, southeastern Pacific Ocean. Micropaleontology 26 (2), 113–150.

Kaiho, K., 1991. Global changes of Paleogene aerobic/anaerobic benthic foraminifera and deep-sea circulation. Palaeogeogr. Palaeoclimatol. Palaeoecol. 83, 65–85.

Kaiho, K., 1994. Benthic foraminiferal dissolved-oxygen index and dissolved-oxygen levels in the modern ocean. Geology 22, 719–722.

Khripounoff, A., Vangriesheim, A., Babonneau, N., Crassous, P., Dennielou, P., Savoye, B., 2003. Direct observation of intense turbidity current activity in the Zaire submarine valley at 4000 m water depth. Mar. Geol. 194 (3–4), 151–158.

Klaucke, I., Hesse, R., Ryan, W.B.F., 1998. Seismic stratigraphy of the Northwest Atlantic Mid-Ocean Channel: growth pattern of a mid-ocean channel–levee complex. Mar. Pet. Geol. 15, 575–585.

Komar, P.D., 1969. The channelized flow of turbidity currents with application to Monterey deep-sea fan channel. J. Geophys. Res 74, 4544–4557.

Lamy, F., Hebbeln, D., Wefer, G., 1998. Terrigenuous sediment supply along the Chilean continental margin: modern regional patterns of texture and composition. Geol. Rundsch. 87, 477–494.

Laursen, J., Normark, W.R., 2002. Late Quaternary Evolution of the San Antonio Submarine Canyon in the central Chile forearc (~33°S). Mar. Geol. 188, 365–390.

Martin, M.W., Kato, T.T., Rodriguez, C., Godoy, E., Duhart, P., McDonough, M., Campos, A., 1999. Evolution of the late Paleozoic accretionary complex and overlying forearc-magmatic arc, south central Chile (38 degrees–41 degrees S): constraints for the tectonic setting along the southwestern margin of Gondwana. Tectonics 18 (4), 582–605.

Martinson, D.G., Pisias, N.G., Hays, J.D., Imbrie, J., Moore, T.C., Shackleton, N.J., 1987. Age dating and the orbital theory of the Ice Ages — development of a high-resolution-0 to 300,000-year chronostratigraphy. Quat. Res. 27 (1), 1–29.

Mix, A.C., Tiedemann, R., Blum, P., et al., 2003. Ocean Drilling Program Proceedings. Initial Reports, vol. 202. (Ocean Drilling Program), College Station, TX. doi:10.2973/odp.proc.ir.202.2003.

Moore, J.C., Watkins, J.C., 1982. Facies belts of the Middle America Trench and forearc region, southern Mexico. Results from Leg 66 DSDP. In: Leggett, J.K. (Ed.), Trench-forearc geology. Spec. Publ. - Geol. Soc. Lond., vol. 10, pp. 77–94.

Muck, M.T., Underwood, M.B., 1990. Upslope flow of turbidity currents: a comparison among field observations, theory, and laboratory models. Geology 18, 54–57.

Mulder, T., Alexander, J., 2001. The physical character of subaqueous sedimentary density flows and their deposits. Sedimentology 48 (2), 269–299.

Nakajima, T., Kanai, Y., 2000. Sedimentary features of seismoturbidites triggered by the 1983 and older historical earthquakes in the eastern margin of the Japan Sea. Sediment. Geol. 135, 1–19.

New, M.G., Hulme, M., Jones, P.D., 1999. Representing 20th century space–time climate variability. I: Development of a 1961–1990 mean monthly terrestrial climatology. J. Climate. 12, 829–856.

Pardo-Casas, F., Molnar, P., 1987. Relative motion of the Nazca (Farallon) and South American Plates since late Cretaceous time. Tectonics 6 (3), 233–248.

Piper, D.J.W., Savoye, B., 1993. Processes of late Quarternary turbidity current flow and deposition on the Var deep-sea fan, north west Mediterranean Sea. Sedimentology 40, 557–582.

Piper, D.J.W., Shor, A.N., Hughes-Clarke, J.E., 1988. The 1929 Grand Banks earthquake, slump and turbidity current. Spec. Pap. - Geol. Soc. Am. 229, 77–92.

Piper, D.J.W., Shaw, J., Skene, K.I., 2007. Stratigraphic and sedimentological evidence for late Wisconsinan sub-glacial outburst floods to Laurentian Fan. Palaeogeogr. Palaeoclimatol. Palaeoecol. 246, 101–119.

Pirmez, C., Imran, J., 2003. Reconstruction of turbidity currents in Amazon Channel. Mar. Pet. Geol. 20, 823–849.

Rabassa, J., Clapperton, C.M., 1990. Quarternary glaciations of the southern Andes. Quat. Sci. Rev. 9, 153–174.

Ranero, C.R., von Huene, R., Weinrebe, W., Reichert, C., 2006. Tectonic processes along the Chile convergent margin. In: Oncken, O., et al. (Ed.), The Andes — Active Subduction Orogeny. Frontiers in Earth Sciences. Springer, Berlin, pp. 91–123.

Rauch, K., 2005. Cyclicity of Peru–Chile Trench sediments between 36° and 38°S: a footprint of paleoclimatic variations? Geophys. Res. Lett. 32 (8), L08302.

Rehak, K., Strecker, M.R., Echtler, H.P., 2008. Morphotectonic segmentation of an active forearc, 37°–41°S, Chile. Geomorphology 94, 98–116.

Reichert, C., SPOC Scientific Shipboard Party Leg-2/3, 2002. Subduction processes off Chile: preliminary geophysical results of SONNE cruise SO-161(2 + 3). In: European Geophysical Society, XXVII General Assembly, Nice, France.

Rothwell, R.G., Thomson, J., Kähler, G., 1998. Low-sea-level emplacement of a very large Late Pleistocene 'megaturbidite' in the western Mediterranean Sea. Nature 392, 377–380.

Schmiedl, G., Hemleben, C., Keller, J., Segl, M., 1998. Impact of climatic changes on the benthic foraminiferal fauna in the Ionian Sea during the last 330,000 years. Paleoceanography 13, 447–458.

Shackleton, N., Duplessy, J., Arnold, M., Maurice, P., Hall, M., Cartlidge, J., 1988. Radiocarbon age of last glacial Pacific deep water. Nature 335, 708–711.

Shepard, F.P., Marshall, N.F., McLoughlin, P.A., Sullivan, G.G., 1979. Currents in Submarine Canyons and other Seavalleys. . AAPG Studies in Geology, vol. 8. American Association of Petroleum Geologists, Tulsa, Oklahoma. 171 pp.

Shiki, T., Kumon, F., Inouchi, Y., Kontani, Y., Sakamoto, S., 2000. Sedimentary features of the seismo-turbidites, Lake Biwa, Japan. Sediment. Geol. 135, 37–50.

Spiess, V., 1993. Digitale Sedimentechographie- Neue Wege zu einer hochauflösenden Akustostratigraphie. Berichte, Fachbereich Geowissenschaften, Universität Bremen, 35, 199 pp. (thesis).

Stuiver, M., Reimer, P.J., Reimer, R.W., 2005. CALIB radiocarbon calibration, 14CHRONO Cent., Queens Univ.Belfast, Belfast, U.K. (Available at http://calib.qub.ac.uk/calib).

Thornburg, T.M., Kulm, L.D., 1990. Submarine-fan development in the southern Chile Trench: a dynamic interplay of tectonics and sedimentation. Geol. Soc. Amer. Bull. 102, 1658–1680.

Underwood, M.B., 1987. Empirical evidence of for upslope flow of turbidity currents in the Aleutian forearc. Abstr. Programs - Geol. Soc. Am. 19, 874.

Völker, D., Weinrebe, W., 2006. Submarine landslides on the continental rise of Central and Southern Chile (32°S–45°S): quantitative description and relation to the segmentation of the margin. EOS Trans. AGU, Fall Meet. Suppl., Abstract OS43C-0658, vol. 87(52).

Völker, D., Wiedicke, M., Ladage, S., Gaedicke, C., Reichert, C., Rauch, K., Kramer, W., Heubeck, C., 2006. Latitudinal variation in sedimentary processes in the Peru–Chile Trench off Central Chile. In: Oncken, O., et al. (Ed.), The Andes — Active Subduction Orogeny. Frontiers in Earth Sciences. Springer, Berlin, pp. 193–216.

Wachter, E., Hayes, J.M., 1985. Exchange of oxygen isotopes in carbon–dioxide–phosphoric acid systems. Chem. Geol. 52, 365–374.

Wentworth, C.K., 1922. A scale of grade and class terms for clastic sediments. J. Geol. 30, 377–392.

Wessel, P., Smith, W.H.F., 1998. New, improved version of the Generic Mapping Tools released. EOS Trans. AGU, vol. 79, p. 579.

Wiedicke, M., shipboard party, 2002. Cruise Report of SONNE cruise 161–5, Bundesanstalt für Geowissenschaften und Rohstoffe Hannover.

Willner, A.P., 2005. Pressure–temperature evolution of a Late Palaeozoic paired metamorphic belt in north-central Chile (34 degrees–35 degrees 30 ′ S). J. Petrol. 46 (9), 1805–1833.

WOCE, 2002. WOCE Global Data, Version 3.0, WOCE International Project Office, WOCE Report No. 180/02, Southampton, UK.